Intensity and Degree of Coherence of Vortex Beams in Atmospheric Turbulence

Gökçe, Muhsin Caner; Baykal, Yahya; Gercekcioglu, Hamza; Ata, Yalcin

DOI
10.1109/JQE.2024.3484248

Publication date
2024

Document Version
Final published version

Published in
IEEE Journal of Quantum Electronics

Intensity and Degree of Coherence of Vortex Beams in Atmospheric Turbulence

Muhsin Caner Gökçe, Yahya Baykal, Hamza Gerçekcioğlu, and Yalçın Ata, *Senior Member, IEEE*

***Abstract*— We utilize the Huygens-Fresnel principle to derive the mutual coherence function (MCF) for a vortex beam, which is the main focus of our investigation. Then, we examine the intensity and modulus of the complex degree of coherence (DOC) characteristics of vortex beams in atmospheric turbulence. Our results indicate that as the topological charge increases, the intensity distribution of the vortex beam becomes less affected by atmospheric turbulence. However, the modulus of the complex DOC decreases.**

***Index Terms*— Atmospheric turbulence, complex degree of coherence, intensity, optical wave propagation, vortex beam.**

I. Introduction

UTILIZATION of vortex beams in optical systems offers numerous benefits because of their possession of orbital angular momentum (OAM) and spiral phase front. These attributes lead to increased information capacity in optical communication systems, improved resolution and sensitivity in microscopy applications, mitigation of atmospheric turbulence effects, and enhanced security in quantum communication [1].

When a laser beam propagates through the atmosphere, it experiences different phenomena such as absorption, scattering, and atmospheric turbulence. These factors lead to signal attenuation and fluctuations upon reception, ultimately diminishing the performance of optical systems. Signal attenuation resulting from absorption and scattering can be mitigated by utilizing specific optical wavelengths within the electromagnetic spectrum. Optimal results are often achieved by selecting wavelengths within the near-infrared range, typically around 1.55 micrometers, which exhibit reduced attenuation due to absorption and scattering effects [2], [3]. Additionally, employing multiple-input multiple-output (MIMO) techniques can help counteract attenuation in optical systems operating in the atmosphere [4], [5].

Received 14 May 2024; revised 10 September 2024; accepted 14 October 2024. Date of publication 21 October 2024; date of current version 31 October 2024. *(Corresponding author: Muhsin Caner Gökçe.)*

Muhsin Caner Gökçe is with the Department of Electrical-Electronics Engineering, TED University, Çankaya, Ankara, 06420 Türkiye, and also with the Department of Geoscience and Remote Sensing, Delft University of Technology, 2628 CD Delft, The Netherlands (e-mail: muhsin.gokce@tedu.edu.tr).

Yahya Baykal is with the Department of Electrical-Electronics Engineering, Çankaya University, 06790 Ankara, Türkiye (e-mail: y.baykal@cankaya.edu.tr).

Hamza Gerçekcioğlu is with the Ministry of Transport and Infrastructure, 06100 Ankara, Türkiye (e-mail: hgercekcioglu@hotmail.com).

Yalçın Ata is with the Department of Electrical and Electronics Engineering, OSTIM Technical University, Yenimahalle, 06374 Ankara, Türkiye (e-mail: ylcnata@gmail.com).

Color versions of one or more figures in this article are available at https://doi.org/10.1109/JQE.2024.3484248.

Digital Object Identifier 10.1109/JQE.2024.3484248

Optical turbulence, on the other hand, is a stochastic and random phenomenon arising from unpredictable fluctuations in the refractive index of the Earth's atmosphere. These fluctuations cause from variations in temperature and wind velocity. Optical turbulence presents challenges by altering the characteristics of the propagating optical beam, resulting in phenomena such as beam spreading and wandering, scintillation, and changes in spatial coherence. In addressing the challenges introduced by optical turbulence, optical systems utilize diverse mitigation techniques such as adaptive optics, spatial diversity, channel coding, and beam shaping [4], [5]. Particularly, beam shaping has emerged as an effective strategy for mitigating turbulence effects. Therefore, the generation of vortex beams has garnered significant attention from researchers [6], [7], [8].

The literature documents the changes in the properties of propagating vortex beams. For example, [9] examines the speckle size of optical vortex and perfect optical vortex using a Fresnel diffraction scheme. Reference [10] studies the spreading of partially coherent flat-topped vortex beams in non-Kolmogorov turbulence, while [11] delves into the propagation and focusing properties of vortex beams through light ray tracing. Additionally, [12] presents findings on the propagation of partially coherent vortex beams. A similar study is conducted experimentally in [13]. The spectral density of partially coherent vortex beams is experimentally analyzed using a spatial light modulator [14]. More recently, the cross-correlation characteristics of the OAM speckles resulting from a scattering medium are studied [15].

In addition, Gbur and Tyson studied the propagation of vortex beams in atmospheric turbulence and found notable results, showing that the topological charge remains highly stable, allowing it to be transmitted across considerable distances without significant loss [16]. They further noted that the topological charge could potentially be utilized as an information carrier in optical communication systems. Additionally, a numerical simulation model of vector vortex beams has been presented in [17]. The study calculates the irradiance pattern, degree of polarization, and scintillation index of a radially polarized beam over various propagation distances in atmospheric conditions, considering both weak and strong turbulence scenarios. Lukin et al. [18] numerically analyzed the spreading of vortex beams and found that, in a randomly inhomogeneous medium, average vortex beams experience less broadening than Gaussian beams. Hricha et al. [19] analytically explored the propagation behavior of partially coherent vortex cosine hyperbolic-Gaussian beams in the atmosphere.

They found that the beam retains its original hollow dark profile over short distances but eventually transitions into a solid Gaussian-like beam in the far-field region. Ebrahim et al. investigated the propagation characteristics of a general model vortex higher-order Cosh-Gaussian beam in atmospheric turbulence [20]. The study demonstrates that the beams maintain their intensity over long propagation distances, making them suitable for long-distance free-space optical communication applications. In a recent study [21], an experimental investigation is conducted to examine the propagation properties of the Laguerre-Gaussian beam, focusing on its intensity distribution, phase pattern, and singularity characteristics. The study reported that the beam quality of the Laguerre-Gaussian beam is superior to the beam quality of the Gaussian beam.

This paper presents an analytical derivation of the MCF of optical vortex beams in atmospheric turbulence. Subsequently, we evaluate the average received intensity and the modulus of the complex degree of coherence (DOC). We employ a Matlab program to explore variations in these optical entities across different optical system parameters, including topological charge, source size, wavelength, propagation distance, and atmospheric structure constant. It should be noted that the average received intensity serves as a key metric for assessing the overall performance of optical systems. Additionally, the modulus of the complex DOC provides valuable insights into the coherence level among distinct points within an optical field. It quantifies the correlation between electric fields at different spatial locations, indicating the spatial properties of the optical system.

We want to highlight that we have developed an analytical solution for the MCF of the vortex beam based on Hermite polynomials. As far as we are aware, there has not been a comprehensive investigation into the modulus of the complex DOC of the vortex beam. We anticipate that the results outlined in this paper will offer practical benefits for a range of optical applications, spanning imaging, interferometry, spectroscopy, metrology, quantum optics, and optical communication systems.

The structure of the paper is outlined as follows: Section II introduces the expressions for received intensity and the modulus of the complex DOC. Section III offers numerical results for these expressions. Finally, Section IV presents the conclusions.

II. Formulation

A. Received Optical Field

The field expression of the Gaussian-vortex beam in the source plane can be defined as [1], [22]

$$u(\mathbf{s},\phi)=A\exp\left[-\frac{(s_x^2+s_y^2)}{2\alpha_s^2}\right]\left[\frac{\sqrt{(s_x^2+s_y^2)}}{\alpha_s^2}\right]^m\exp(jm\phi), \quad (1)$$

where A is the amplitude, α_s is the size of the Gaussian beam, $\mathbf{s}=(s_x,s_y)$ is the transmitter plane spatial coordinates, m is the topological charge, $j=\sqrt{-1}$, and $\phi=\arctan(s_y/s_x)$ is the azimuthal angle. It is worth mentioning that when m equals zero in Eq. (1), it represents a pure Gaussian beam.

According to [23], the last two terms of Eq. (1) can be expressed as

$$\left[\frac{\sqrt{(s_x^2+s_y^2)}}{\alpha_s^2}\right]^m\exp(jm\phi)=\sum_{m_0=0}^{m}\frac{j^{m_0}}{(2\alpha_s)^m}\binom{m}{m_0}\times H_{m-m_0}(s_x)H_{m_0}(s_y), \quad (2)$$

where $H_m(.)$ is the Hermite polynomial of order m, and $\binom{m}{m_0}$ is the binomial coefficient. Upon substitution of Eq. (2) into Eq. (1), we derive the source field expression eliminating any dependence on ϕ.

$$u(\mathbf{s})=\exp\left[-\frac{(s_x^2+s_y^2)}{2\alpha_s^2}\right]\sum_{m_0=0}^{m}\frac{Aj^{m_0}}{(2\alpha_s)^m}\binom{m}{m_0}\times H_{m-m_0}(s_x)H_{m_0}(s_y). \quad (3)$$

As mentioned in reference [24], the Huygens-Fresnel integral yields the optical field after it has traversed a turbulent atmosphere

$$u(\mathbf{p},L)=A\frac{k\exp(jkL)}{2\pi jL}\int_{-\infty}^{\infty}\int_{-\infty}^{\infty}u(\mathbf{s},\phi)\times\exp\left\{\frac{jk}{2L}\left[(s_x-p_x)^2+(s_y-p_y)^2\right]\right\}\times\exp[\psi(\mathbf{s},\mathbf{p})]ds_xds_y, \quad (4)$$

where $\mathbf{p}=(p_x,p_y)$ is the receiver plane spatial coordinate, $k=2\pi/\lambda$ denotes the wavenumber, λ is the wavelength of the optical beam, L is the propagation distance, $\psi(\mathbf{s},\mathbf{p})$ signifies the random complex phase of a spherical wave while it propagates from the source point to the receiver point.

B. Mutual Coherence Function

The MCF, known by several terms like cross-spectral density, second-order moment, and field correlation in literature, is employed to determine the modulus of the complex DOC, which characterizes the decay of spatial coherence in an initially coherent wave. Additionally, it aids in computing various aspects of the optical beam such as mean irradiance, spot size, beam wander, spatial coherence width, root mean square (RMS) angle of arrival (AOA), and image jitter [25].

The MCF for a vortex beam is defined by [25]

$$\Gamma(\mathbf{p}_1,\mathbf{p}_2,L)=\left\langle u(\mathbf{p}_1,L)u^*(\mathbf{p}_2,L)\right\rangle, \quad (5)$$

where $\mathbf{p}_1$ and $\mathbf{p}_2$ represent the points of observation within the receiver plane, $*$ denotes the complex conjugate, $\langle.\rangle$ shows the ensemble average over the turbulence statistics. Substituting Eq. (4) into Eq. (5), we obtain

$$\Gamma(p_1,p_2)=\frac{A^2}{(\lambda L)^2}\times\int_{-\infty}^{\infty}\int_{-\infty}^{\infty}u(\mathbf{s}_1,\phi)\times\exp\left\{\frac{jk}{2L}\left[(s_{1x}-p_{1x})^2+(s_{1y}-p_{1y})^2\right]\right\}\mathrm{d}s_{1x}\mathrm{d}s_{1y}$$

$$\times \int_{-\infty}^{\infty}\int_{-\infty}^{\infty} u^*(\mathbf{s}_2,\phi) \times \exp\left\{-\frac{jk}{2L}\left[(s_{2x}-p_{2x})^2+(s_{2y}-p_{2y})^2\right]\right\} \mathrm{d}s_{2x}\mathrm{d}s_{2y} \times \left\langle \exp\left[\psi(\mathbf{s}_1,\mathbf{p}_1)+\psi^*(\mathbf{s}_2,\mathbf{p}_2)\right]\right\rangle, \quad (6)$$

where the final line in Eq. (6) is determined by [26]

$$\begin{aligned}&\left\langle \exp\left[\psi(\mathbf{s}_1,\mathbf{p}_1)+\psi^*(\mathbf{s}_2,\mathbf{p}_2)\right]\right\rangle \\ &= \exp\left[-\frac{1}{\rho_0^2}\left(|s_1-s_2|^2+|s_1-s_2|.|p_1-p_2|+|p_1-p_2|^2\right)\right] \\ &= \exp\left\{-\frac{1}{\rho_0^2}\left[(s_{1x}-s_{2x})^2+(s_{1y}-s_{2y})^2\right.\right. \\ &\quad +(s_{1x}-s_{2x})(p_{1x}-p_{2x})+(s_{1y}-s_{2y})(p_{1y}-p_{2y}) \\ &\quad \left.\left.+(p_{1x}-p_{2x})^2+(p_{1y}-p_{2y})^2\right]\right\}, \end{aligned} \quad (7)$$

where ρ_0 represents the spatial coherence length of a spherical wave and is specified as [27]

$$\rho_0 = \left(0.546C_n^2k^2L\right)^{-3/5}, \quad (8)$$

where C_n^2 is the structure constant of the atmosphere. By inserting Eq. (7) and Eq. (3) into Eq. (6) and subsequently solving the integral, the mutual coherence function of the vortex beam is found to be

$$\begin{aligned}&\Gamma(p_1,p_2) \\ &= \left\langle u(p_1,L)u^*(p_2,L)\right\rangle \\ &= \exp\left\{-\frac{1}{\rho_0^2}\left[(p_{1x}-p_{2x})^2+(p_{1y}-p_{2y})^2\right]\right\} \\ &\quad \times \exp\left[\frac{jk}{2L}\left(p_{1x}^2-p_{2x}^2+p_{1y}^2-p_{2y}^2\right)\right] \\ &\quad \times \frac{A^2}{(\lambda L)^2}\sum_{m_0=0}^{m}\sum_{m_1=0}^{m}\frac{1}{(2\alpha_s)^{2m}}j^{m_0}(-j)^{m_1}\binom{m}{m_0}\binom{m}{m_1} \\ &\quad \times F_x(p_1,p_2)F_y(p_1,p_2), \end{aligned} \quad (9)$$

where

$$\begin{aligned}&F_x(p_1,p_2) \\ &= \sum_{p=0}^{(m-m_1)/2}\sum_{k=0}^{(m-m_1-2p)}\sum_{q=0}^{(m-m_0)/2}\sum_{w=0}^{(m-m_1-2p-k)/2} \\ &\quad \times (-\pi)(-1)^{(3m-2m_1-p-k-m_0+w+q)}2^{-(m-m_1-2p)/2} \\ &\quad \times \frac{(m-m_1-2p)!}{(m-m_1-2p-k)!k!}\frac{(m-m_1)!}{(m-m_1-2p)!p!} \\ &\quad \times \frac{(m-m_0)!}{(m-m_0-2q)!q!}\frac{(m-m_1-2p-k)!}{(m-m_1-2p-k-2w)!w!} \\ &\quad \times \left(\frac{j}{\sqrt{C_1}}\right)^{(1+m-m_1-2p)}\left(\frac{jE}{\sqrt{2C_1}}\right)^{(m-m_1-2p-k-2w)} \\ &\quad \times \left(\frac{j}{\sqrt{K}}\right)^{(1+m-m_0+m-m_1-2p-k-2q-2w)} \\ &\quad \times \exp\left(\frac{D_x^2}{4C_1}+\frac{G_x^2}{4K}\right)H_k\left(\frac{jD_x}{\sqrt{2C_1}}\right) \\ &\quad \times \mathrm{H}_{(m-m_0+m-m_1-2p-k-2q-2w)}\left(\frac{jG_x}{2\sqrt{K}}\right), \end{aligned} \quad (10)$$

where $C_1=\frac{1}{2\alpha_s^2}+\frac{jk}{2L}+\frac{1}{\rho_0^2}$, $K=\left(B_1-\frac{E^2}{4C_1}\right)$, $E=\frac{2}{\rho_0^2}$, $B_1=\frac{1}{2\alpha_s^2}-\frac{jk}{2L}+\frac{1}{\rho_0^2}$, $D_x=2p_{2x}\frac{jk}{2L}+\frac{1}{\rho_0^2}(p_{1x}-p_{2x})$, $G_x=\frac{2D_xE}{4C_1}-B_{2x}$, $B_{2x}=2p_{1x}\frac{jk}{2L}+\frac{1}{\rho_0^2}(p_{1x}-p_{2x})$. Note that to derive F_y, replace D_x, G_x, B_{2x}, $(m-m_0)$ and $(m-m_1)$ in Eq. (10) with D_y, G_y, B_{2y}, m_0 and m_1, respectively. Then, substitute p_{1x} and p_{2x} by p_{1y} and p_{2y}, respectively. The steps of the derivation are outlined in Appendix A. It is crucial to note that the upper limit of all summation indices in the formulas must be truncated to the floor value to ensure accurate results [28]. Additionally, it is worth mentioning that in order to solve Eq. (6), we utilize the integral formulas that we derived [27]

$$\begin{aligned}&\int_{-\infty}^{\infty}dx\,H_n(x)\exp\left(-ax^2\mp bx\right) \\ &\quad = (-1)^{(n)}(-j)\sqrt{\pi}\exp\left(\frac{b^2}{4a}\right) \\ &\quad \times \sum_{n_0=0}^{n/2}\frac{n!}{(n-2n_0)!n_0!}(-1)^{n_0} \\ &\quad \times \left(\frac{j}{\sqrt{a}}\right)^{(1+n-2n_0)}\mathrm{H}_{(n-2n_0)}\left(\frac{jb}{2\sqrt{a}}\right), \end{aligned} \quad (11)$$

$$\begin{aligned}&\int_{-\infty}^{\infty}dx\,H_y(ax)H_u(bx)\exp\left(-cx^2\mp fx\right) \\ &\quad = (-1)^{(u+y)}(-j)\sqrt{\pi}\exp\left(\frac{f^2}{4c}\right) \\ &\quad \times \sum_{q=0}^{y/2}\sum_{w=0}^{u/2}\frac{y!}{(y-2q)!q!}\frac{u!}{(u-2w)!w!}(-1)^{w+q} \\ &\quad \times \left(\frac{j}{\sqrt{c}}\right)^{(1+y+u-2q-2w)}a^{(y-2q)}b^{(u-2w)} \\ &\quad \times \mathrm{H}_{(y+u-2q-2w)}\left(\frac{jf}{2\sqrt{c}}\right), \end{aligned} \quad (12)$$

$$H_n(z_1+z_2) = 2^{-\frac{n}{2}}\sum_{k=0}^{n}\binom{n}{k}H_k\left(z_1\sqrt{2}\right)H_{n-k}\left(z_2\sqrt{2}\right). \quad (13)$$

We note that the formula we derived in Eq. (11) accurately aligns with the specific case of the formula presented by Belafhal et al. in Eq. (2) of [28].

C. Optical Intensity at Receiver

The received intensity of vortex beam can be found using the MCF of incident field at identical observation points $\mathbf{p}_1=\mathbf{p}_2=\mathbf{p}$ [25]

$$\langle I(\mathbf{p},L)\rangle = \Gamma(\mathbf{p},\mathbf{p},L) = \left\langle u(\mathbf{p},L)u^*(\mathbf{p},L)\right\rangle, \quad (14)$$

and thus the intensity is given by

$$\langle I(\mathbf{p},L)\rangle = \frac{A^2}{(\lambda L)^2}\sum_{m_0=0}^{m}\sum_{m_1=0}^{m}\frac{1}{(2\alpha_s)^{2m}}j^{m_0}(-j)^{m_1} \times \binom{m}{m_0}\binom{m}{m_1}F_xF_y. \quad (15)$$

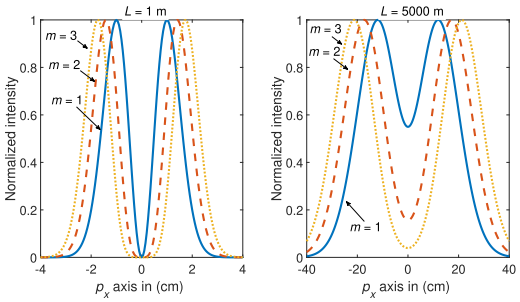

Fig. 1. Normalized intensity distribution of the vortex beam both near its source and as it passes through atmospheric turbulence, depicted in two dimensions $p_y = 0$, showcasing different topological charge values at propagation distances of both 1 m and 5000 m for $\alpha_s = 1$ cm, $\lambda = 1.55$ μm, $C_n^2 = 5 \times 10^{-15}\mathrm{m}^{-2/3}$.

It is important to highlight that because the observation points are identical $\mathbf{p}_1 = \mathbf{p}_2 = \mathbf{p}$ the expressions D_x and B_{2x} in Eq. (10) are adjusted to $D_x = B_{2x} = 2p_x \frac{jk}{2L}$

D. Complex Degree of Coherence

The degradation in spatial coherence within an initially coherent vortex beam, from one position $\mathbf{p}_1$ to another $\mathbf{p}_2$ or vice versa, can be deduced by analyzing the modulus of the complex degree of coherence [25]

$$\mu(\mathbf{p}_1, \mathbf{p}_2, L) = \frac{|\Gamma(\mathbf{p}_1, \mathbf{p}_2, L)|}{\sqrt{\Gamma(\mathbf{p}_1, \mathbf{p}_1, L)}\sqrt{\Gamma(\mathbf{p}_2, \mathbf{p}_2, L)}}. \tag{16}$$

It should be noted that μ takes values between 0 and 1. A magnitude of 1 signifies perfect coherence, indicating complete correlation between the fields at the two points. Conversely, a magnitude of 0 denotes total incoherence, indicating no correlation between the fields. Magnitudes between 0 and 1 indicate partial coherence, reflecting a degree of correlation between the fields. The exact analytical expression for μ is given in Eq. (B.1) of Appendix B.

The modulus of the complex degree of coherence μ is commonly used in various optical applications, including imaging, interferometry, and optical communication systems.

III. Numerical Results

In this section, we investigate the simulation of a vortex beam passing horizontally through atmospheric turbulence. Focusing on Figures 1-3, we present the normalized optical intensity at the observation plane under various parameters. Note that the normalized optical intensity is calculated as the ratio of the average intensity $I(\mathbf{p}, L)$ to the maximum value of the average intensity $I(\mathbf{p}, L)_{\max}$. Additionally, Figures 4-10 showcase the modulus of the complex degree of coherence of the vortex beam. It is important to mention that in Fig. 4 and Fig. 5, the horizontal axis represents the diagonal distance, calculated as $\left(p_{2x}^2 + p_{2y}^2\right)^{0.5}$. Furthermore, when m equals zero, the vortex beam transforms into a pure Gaussian beam.

Fig. 1 illustrates the normalized intensity of the vortex beam at distances $L = 1$ m and $L = 5000$ m plotted against the receiver coordinate p_x for various topological charge m values. The system parameters are set with a laser beam source size

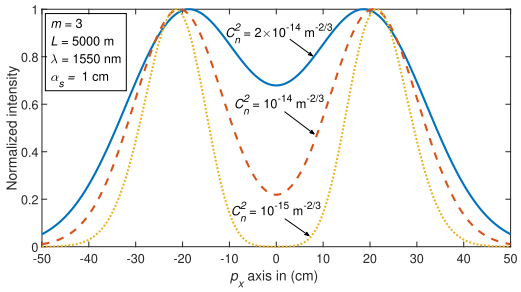

Fig. 2. Normalized intensity distribution of the vortex beam in atmospheric turbulence, analyzed in two dimensions along p_x axis, is illustrated for different values of the structure constant C_n^2 with $m = 3$.

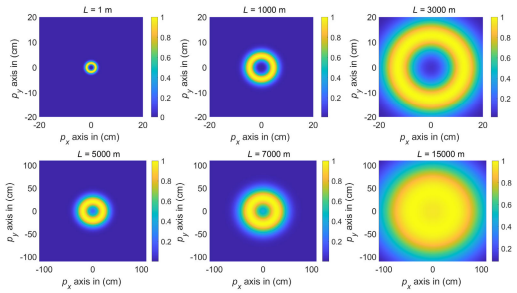

Fig. 3. Normalized intensity profile of the vortex beam passing through the atmospheric turbulence versus the different propagation distances for $\alpha_s = 1$ cm, $m = 3$, $\lambda = 1.55$ μm, $C_n^2 = 10^{-14}\mathrm{m}^{-2/3}$.

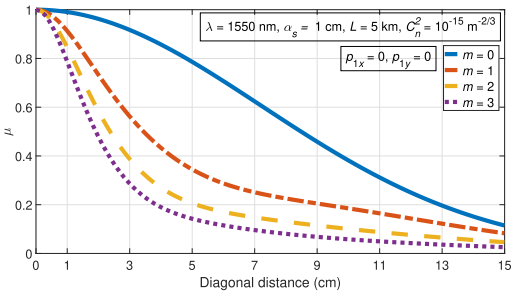

Fig. 4. Complex DOC of vortex beam versus diagonal distance for various topological charge m values.

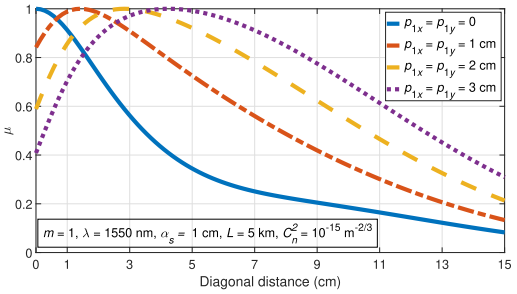

Fig. 5. Complex DOC of vortex beam versus diagonal distance for various $\mathbf{p}_1$ values with a fixed topological charge $m = 1$.

of $\alpha s = 1$ cm, a laser wavelength of $\lambda = 1.55$ μm, and the atmospheric structure constant of $C_n^2 = 5 \times 10^{-15}\mathrm{m}^{-2/3}$. Near the source, at $L = 1$ m where turbulence is negligible, the on-axis intensities for all cases are zero. However, when the propagation distance is taken to be $L = 5000$ m, the on-axis intensities deviate from zero. It can be inferred that turbulence has a lesser effect on vortex beams with higher topological

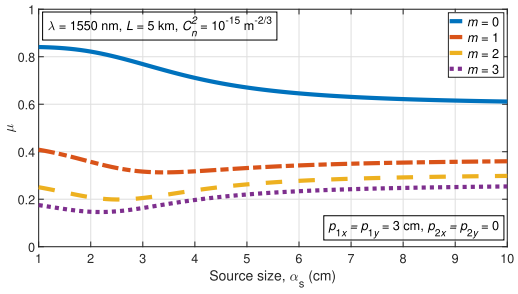

Fig. 6. Complex DOC of vortex beam versus source size α_s for various topological charge m values.

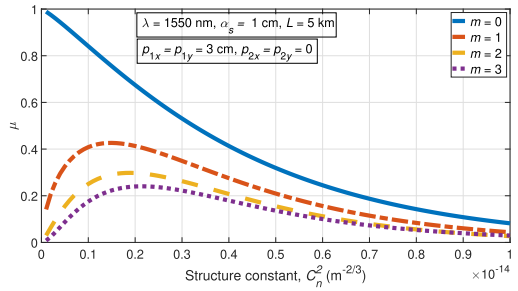

Fig. 7. Complex DOC of vortex beam versus structure constant C_n^2 for various topological charge m values.

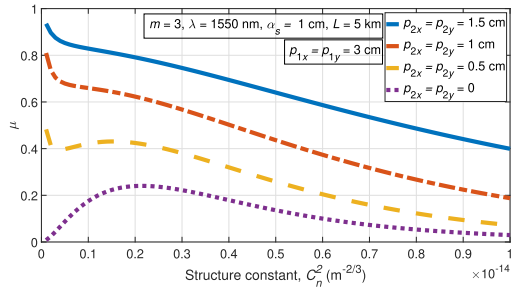

Fig. 8. Complex DOC of vortex beam versus structure constant C_n^2 for various $\mathbf{p}_2$ values for topological charge $m = 3$.

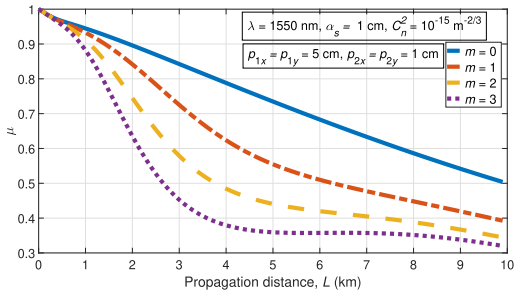

Fig. 9. Complex DOC of vortex beam versus propagation distance L for various topological charge m values.

charges. In other words, vortex beams with higher topological charges are more resistant to atmospheric turbulence because their centers fill up more slowly in comparison. In Fig. 2, similar to Fig. 1, the plot showcases the relationship between normalized intensity and p_x at $L = 5000$m for different values of the structure constant C_n^2 for a fixed topological charge $m = 3$. The p_y axis is set to zero in the simulation. From Fig. 2, it can be noted that with an increase in turbulence level, indicated by higher values of the structure constant,

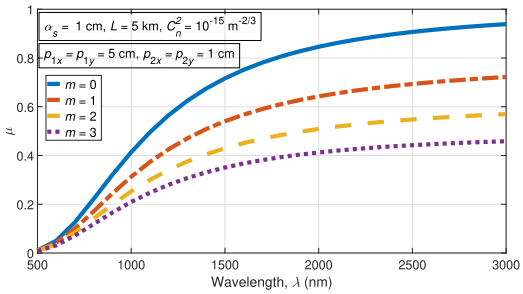

Fig. 10. Complex DOC of vortex beam versus wavelength λ of the source for various topological charge m values.

the center of the curve starts to elevate. These results are expected because, at high levels of atmospheric turbulence, any beam shape generally starts to evolve into a Gaussian-like profile [20].

In Fig. 3, the influence of atmospheric turbulence on the vortex beam is depicted across various propagation distances L, with parameters held constant at $\alpha_s = 1$ cm, $m = 3$, $\lambda = 1.55$ μm, $C_n^2 = 10^{-14}\text{m}^{-2/3}$. It is found that initially $L = 1$ m, the vortex beam has zero intensity along its axis and appears smaller footprint compared to others. However, as the propagation distance L increases, the hole in the middle of the beam becomes filled with intensity, and the beam size also enlarges. Eventually, at very long distances, the beam presents a Gaussian-like profile. These results indicate that both atmospheric turbulence and propagation distance are vital in determining the intensity distribution at the beam's center.

In Fig. 4, the modulus of the complex degree of coherence μ is plotted against the diagonal distance from the origin of the receiver plane for various topological charge m values. Additionally, the selection of $\mathbf{p}_1$ is on the axis specifically with $p_{1x} = 0$, $p_{1y} = 0$. It has been observed that as the diagonal distance increases, the modulus of the complex degree of coherence μ decreases. This result is expected since we are comparing the on-axis field with the field at a diagonal distance originating from the center. When the diagonal distance is zero, we are comparing the same points, causing μ to reach its maximum value. As the diagonal distance increases, the correlation between the fields decreases. Additionally, μ also decreases with an increase in the topological charge m. In Fig. 5, the modulus of the complex degree of coherence μ is plotted against the diagonal distance. Here, the topological charge is fixed at $m = 1$, and the impact of observation points $\mathbf{p}_1$ on the parameter μ is examined. It has been observed that as the observation points converge, the maximum values of μ are achieved. Additionally, the peak point of the blue solid curve shifts towards the right as p_{1x} and p_{1y} increase.

In Fig. 6, the impact of changes in the source size α_s on the modulus of the complex degree of coherence μ is illustrated while varying the topological charge m. It is observed that as the source size α_s increases, the parameter μ initially decreases and then stabilizes for the pure Gaussian beam, i.e., $m = 0$. However, for vortex beams with varying topological charges, μ initially decreases and then slightly increases. The physical explanation for this figure is that the increase in field correlation between two points, $\mathbf{p}_1$ and $\mathbf{p}_2$, is smaller

than the increase in the intensity at those points. As a result, the complex degree of coherence, μ, as defined in Eq. (16), initially decreases as the source size increases.

In Fig. 7, the modulus of the complex degree of coherence μ versus structure constant C_n^2. is demonstrated for various topological charge m values. It is found that as C_n^2 increases, the μ value of the Gaussian beam (i.e., $m = 0$) decreases comparatively. However, for vortex beams with different topological charges, the pattern differs significantly. With increasing C_n^2, μ initially increases before decreasing. In Fig. 8, akin to Fig. 7, the plot illustrates the modulus of the complex degree of coherence μ versus the structure constant C_n^2. However, in Fig. 8, the topological charge is set to $m = 3$, and the impact of different observation points $\mathbf{p}_2$ on μ is examined. General behavior observed from Fig. 8 is that as $\mathbf{p}_2$ approaches $\mathbf{p}_1$, μ increases. Furthermore, when C_n^2 increases, μ generally decreases. However, in the scenario where $p_{2x} = p_{2y} = 0$, μ initially increases before decreasing with the increase in C_n^2.

Fig. 9 displays how the modulus of the complex degree of coherence μ changes with propagation distance L for various topological charge m values. It is evident that as the propagation distance increases, μ decreases as expected. Furthermore, with increasing topological charge, μ also decreases.

In Fig. 10, the graph illustrates the modulus of the complex degree of coherence μ plotted against the wavelength of the light source λ, with different topological charge m values. The overall trend observed in Fig. 10 is that as the wavelength increases, μ increases. Moreover, an increase in the topological charge results in a decrease in μ.

It is important to note that the complex degree of coherence, μ, depends not only on the field correlation between $\mathbf{p}_1$ and $\mathbf{p}_2$ but also on the intensity at these points. In certain cases, both the field correlation and intensity may increase, yet μ can still decrease. As a result, we cannot provide an immediate conclusion about the complex degree of coherence μ without performing the simulation.

IV. Conclusion

The research investigates the intensity properties and the modulus of the complex degree of coherence between two distinct receiver locations in systems employing vortex lasers operating within atmospheric turbulence. The derivation of the mutual coherence function serves as the primary focus for this investigation. The figures presented in the study are generated using the MATLAB program. The study's general findings can be summarized as follows: as the topological charge rises, the intensity distribution of the vortex beam at the observation plane is less influenced by atmospheric turbulence. This trend is clearly depicted in Fig. 1, particularly at $L = 5000$ m. As the structure constant or propagation distance increases, the void in the center of the beam fills with intensity, and the overall size of the beam also expands. Furthermore, if the propagation distance is set to be very large in atmospheric turbulence, the vortex beam transforms into a Gaussian beam. In addition, as the topological charge, diagonal distance, and link distance increase, the modulus of the complex degree of coherence of the vortex beam decreases. Conversely, if the wavelength of the light source increases, the modulus of the complex degree of coherence of the vortex beam increases.

The findings presented in this study will be valuable for optical system designers involved in diverse optical applications, such as imaging, microscopy, interferometry, as well as optical and quantum communications.

Appendix A
MCF Derivations

To derive F_x and F_y in Eq. (9), we apply the following integral expressions.

$$F_x = \int_{-\infty}^{\infty} H_{m-m_0}(s_{1x}) \exp\left\{-s_{1x}^2 B_1 - s_{1x} B_{2x}\right\} \mathrm{d}s_{1x} \times \int_{-\infty}^{\infty} H_{m-m_1}(s_{2x}) \exp\left\{-s_{2x}^2 C_1 + s_{2x} C_{2x}\right\} \mathrm{d}s_{2x}, \quad \text{(A.1)}$$

$$F_y = \int_{-\infty}^{\infty} H_{m_0}(s_{1y}) \exp\left\{-s_{1y}^2 B_1 - s_{1y} B_{2y}\right\} \mathrm{d}s_{1y} \times \int_{-\infty}^{\infty} H_{m_1}(s_{2y}) \exp\left\{-s_{2y}^2 C_1 + s_{2y} C_{2y}\right\} \mathrm{d}s_{2y}, \quad \text{(A.2)}$$

where $C_{2x} = D_x + s_{1x}E$ and $C_{2y} = D_y + s_{1y}E$. It is important to note that solution of F_x is provided in Eq. (10). Here,

$$\mu(\mathbf{p}_1, \mathbf{p}_2, L) = \left| \begin{array}{l} \exp\left[-\frac{1}{\rho_0^2}(p_{1x} - p_{2x})^2\right] \\ \times \exp\left[-\frac{1}{\rho_0^2}(p_{1y} - p_{2y})^2\right] \\ \times \exp\left\{\frac{jk}{2L}\left(p_{1x}^2 - p_{2x}^2 + p_{1y}^2 - p_{2y}^2\right)\right\} \\ \times \sum_{m_0=0}^{m} \sum_{m_1=0}^{m} \frac{j^{m_0}(-j)^{m_1}}{(2\alpha_s)^{2m}} \binom{m}{m_0} \binom{m}{m_1} \\ \times F_x(\mathbf{p}_1, \mathbf{p}_2) F_y(\mathbf{p}_1, \mathbf{p}_2) \end{array} \right| \cdot \left(\begin{array}{l} \frac{A^2}{(\lambda L)^2 (2\alpha_s)^{4m}} \sum_{m_2=0}^{m} \sum_{m_3=0}^{m} \sum_{m_4=0}^{m} \sum_{m_5=0}^{m} j^{m_2+m_4} \\ \times (-j)^{m_3+m_5} \binom{m}{m_2} \binom{m}{m_3} \binom{m}{m_4} \binom{m}{m_5} \\ \times F_x(\mathbf{p}_1, \mathbf{p}_1) F_y(\mathbf{p}_1, \mathbf{p}_1) \\ \times F_x(\mathbf{p}_2, \mathbf{p}_2) F_y(\mathbf{p}_2, \mathbf{p}_2) \end{array} \right)^{-1/2} \quad \text{(B.1)}$$

we provide the solution for F_y

$$F_y(p_1, p_2) = \sum_{p=0}^{m_1/2} \sum_{k=0}^{m_1-2p} \sum_{q=0}^{m_0/2} \sum_{w=0}^{(m_1-2p-k)/2} \times (-\pi)(-1)^{(2m_1-p-k+m_0+w+q)} 2^{-(m_1-2p)/2} \times \frac{(m_1-2p)!}{(m_1-2p-k)!k!} \frac{m_1!}{(m_1-2p)!p!} \times \frac{m_0!}{(m_0-2q)!q!} \frac{(m_1-2p-k)!}{(m_1-2p-k-2w)!w!} \times \left(\frac{j}{\sqrt{C_1}}\right)^{(1+m_1-2p)} \left(\frac{jE}{\sqrt{2C_1}}\right)^{(m_1-2p-k-2w)} \times \left(\frac{j}{\sqrt{K}}\right)^{(1+m_0+m_1-2p-k-2q-2w)} \times \exp\left(\frac{D_y^2}{4C_1} + \frac{G_y^2}{4K}\right) H_k\left(\frac{jD_y}{\sqrt{2C_1}}\right) \times \mathrm{H}_{(m_0+m_1-2p-k-2q-2w)}\left(\frac{jG_y}{2\sqrt{K}}\right), \quad \text{(A.3)}$$

where $D_y = 2p_{2y}\frac{jk}{2L} + \frac{1}{\rho_0^2}(p_{1y} - p_{2y})$, $G_y = \frac{2D_yE}{4C_1} - B_{2y}$, and $B_{2y} = 2p_{1y}\frac{jk}{2L} + \frac{1}{\rho_0^2}(p_{1y} - p_{2y})$.

APPENDIX B
ANALYTICAL FORMULA FOR THE MODULUS OF THE COMPLEX DEGREE OF COHERENCE

By substituting Eq. (9) into Eq. (16) for different observation points, p_1 and p_2, we obtain the modulus of the complex degree of coherence as given in Eq. (B.1), as shown at the bottom of the previous page.

ACKNOWLEDGMENT

Muhsin Caner Gökçe, Yahya Baykal, and Yalçın Ata acknowledge the support provided by TED University, Çankaya University, and OSTİM Technical University, respectively.

REFERENCES

[1] H. Zhang, J. Zeng, X. Lu, Z. Wang, C. Zhao, and Y. Cai, "Review on fractional vortex beam," *Nanophotonics*, vol. 11, no. 2, pp. 241–273, Jan. 2022.
[2] I. I. Kim and E. J. Korevaar, "Availability of free-space optics (FSO) and hybrid FSO/RF systems," *Proc. SPIE*, vol. 4530, pp. 84–95, Nov. 2001.
[3] E. J. Korevaar, I. I. Kim, and B. McArthur, "Atmospheric propagation characteristics of highest importance to commercial free space optics," *Proc. SPIE*, vol. 4976, pp. 1–12, Apr. 2003.
[4] M. A. Khalighi and M. Uysal, "Survey on free space optical communication: A communication theory perspective," *IEEE Commun. Surveys Tuts.*, vol. 16, no. 4, pp. 2231–2258, 4th Quart., 2014.
[5] H. Kaushal and G. Kaddoum, "Optical communication in space: Challenges and mitigation techniques," *IEEE Commun. Surveys Tuts.*, vol. 19, no. 1, pp. 57–96, 1st Quart., 2016.
[6] I. R. Srimathi, Y. Li, W. F. Delaney, and E. G. Johnson, "Subwavelength grating based metal-oxide nano-hair structures for optical vortex generation," *Opt. Exp.*, vol. 23, no. 15, pp. 19056–19065, 2015.
[7] X. Zhang, A. Wang, R. Chen, Y. Zhou, H. Ming, and Q. Zhan, "Generation and conversion of higher order optical vortices in optical fiber with helical fiber Bragg gratings," *J. Lightw. Technol.*, vol. 34, no. 10, pp. 2413–2418, May 15, 2016.
[8] A. S. Ostrovsky, C. Rickenstorff-Parrao, and V. Arrizón, "Generation of the 'perfect' optical vortex using a liquid-crystal spatial light modulator," *Opt. Lett.*, vol. 38, no. 4, pp. 534–536, 2013.
[9] C. H. Acevedo, Y. Torres-Moreno, and A. Dogariu, "Spatial intensity correlations of a vortex beam and a perfect optical vortex beam," *J. Opt. Soc. Amer. A, Opt. Image Sci.*, vol. 36, no. 4, pp. 518–525, 2019.
[10] X. He and B. Lü, "Propagation of partially coherent flat-topped vortex beams through non-Kolmogorov atmospheric turbulence," *J. Opt. Soc. Amer. A, Opt. Image Sci.*, vol. 28, no. 9, pp. 1941–1948, 2011.
[11] M.-Q. Cai, Q. Wang, Y.-N. Li, and C.-H. Tu, "Propagation and focusing properties of vortex beams based on light ray tracing," *Frontiers Phys.*, vol. 10, Jun. 2022, Art. no. 931131.
[12] T. Wang, J. Pu, and Z. Chen, "Beam-spreading and topological charge of vortex beams propagating in a turbulent atmosphere," *Opt. Commun.*, vol. 282, no. 7, pp. 1255–1259, Apr. 2009.
[13] T. Wang, "Propagation of partially coherent vortex beams in a turbulent atmosphere," *Opt. Eng.*, vol. 47, no. 3, Mar. 2008, Art. no. 036002.
[14] Z. Liu and D. Zhao, "Propagation of partially coherent vortex beams in atmospheric turbulence by a spatial light modulator," *Laser Phys. Lett.*, vol. 16, no. 5, May 2019, Art. no. 056003.
[15] R. Ma et al., "Orbital-angular-momentum-dependent speckles for spatial mode sorting and demultiplexing," *Optica*, vol. 11, no. 5, pp. 595–605, 2024.
[16] G. Gbur and R. K. Tyson, "Vortex beam propagation through atmospheric turbulence and topological charge conservation," *J. Opt. Soc. Amer. A, Opt. Image Sci.*, vol. 25, no. 1, pp. 225–230, Jan. 2008.
[17] W. Cheng, J. W. Haus, and Q. W. Zhan, "Propagation of vector vortex beams through a turbulent atmosphere," *Opt. Exp.*, vol. 17, no. 20, pp. 17829–17836, Sep. 2009.
[18] V. P. Lukin, P. A. Konyaev, and V. A. Sennikov, "Beam spreading of vortex beams propagating in turbulent atmosphere," *Appl. Opt.*, vol. 51, no. 10, pp. 84–87, 2012.
[19] Z. Hricha, M. Lazrek, M. E. Halba, and A. Belafhal, "Effect of a turbulent atmosphere on the propagation properties of partially coherent vortex cosine-hyperbolic-Gaussian beams," *Opt. Quantum Electron.*, vol. 54, no. 11, p. 719, Nov. 2022.
[20] A. A. A. Ebrahim, M. A. Swillam, and A. Belafhal, "Atmospheric turbulent effects on the propagation properties of a general model vortex higher-order cosh-Gaussian beam," *Opt. Quantum Electron.*, vol. 55, no. 4, p. 316, Apr. 2023.
[21] Y. Zhang, C. Ke, Y. Xie, and Y. Zhang, "Experimental investigation of LG beam propagating in actual atmospheric turbulence," *Results Phys.*, vol. 35, Apr. 2022, Art. no. 105327.
[22] Y. Cai and S. He, "Propagation of a Laguerre–Gaussian beam through a slightly misaligned paraxial optical system," *Appl. Phys. B, Lasers Opt.*, vol. 84, no. 3, pp. 493–500, Sep. 2006.
[23] I. Kimel and L. R. Elias, "Relations between Hermite and Laguerre Gaussian modes," *IEEE J. Quantum Electron.*, vol. 29, no. 9, pp. 2562–2567, Sep. 1993.
[24] Y. Baykal, Y. Ata, and M. C. Gökçe, "Underwater turbulence, its effects on optical wireless communication and imaging: A review," *Opt. Laser Technol.*, vol. 156, Dec. 2022, Art. no. 108624.
[25] L. C. Andrews and R. L. Phillips, *Laser Beam Propagation Through Random Media*, 2nd ed., Bellingham, WA, USA: SPIE Press, 2005.
[26] M. C. Gökçe, Y. Baykal, and Y. Ata, "Fiber-coupling efficiency of laser array beam from turbulent atmosphere to fiber link," *J. Lightw. Technol.*, vol. 41, no. 1, pp. 59–65, Sep. 6, 2023.
[27] M. C. Gökçe, Y. Baykal, Y. Ata, and H. Gerçekcioğlu, "Multimode beam propagation through atmospheric turbulence," *J. Quant. Spectrosc. Radiat. Transf.*, vol. 314, Feb. 2024, Art. no. 108857.
[28] A. Belafhal, Z. Hricha, L. Dalil-Essakali, and T. Usman, "A note on some integrals involving Hermite polynomials and their applications," *Adv. Math. Mod. Appl.*, vol. 5, no. 3, pp. 313–319, 2020.

Muhsin Caner Gökçe received the M.S. degree in electronics engineering from Ankara University, Ankara, Türkiye, in 2012, and the Ph.D. degree in electronic and communication engineering from Çankaya University, Ankara, in 2016. He is an Associate Professor with the Department of Electrical-Electronics Engineering, TED University, Ankara. He is currently a Post-Doctoral Researcher with the Department of Geoscience and Remote Sensing, Delft University of Technology, The Netherlands. His research interests include optical wireless communication and optical beam propagation through turbulent media.

Yahya Baykal received the Ph.D. degree from the Electrical Engineering and Computer Sciences Department, Northwestern University, Evanston, IL, USA. He is a Professor and the Chairperson with the Department of Electrical-Electronics Engineering, Çankaya University, Ankara, Türkiye. He is the author of more than 220 SCI journal articles and more than 290 publications. His research interests include optical communication, optical wave propagation in atmospheric, underwater media, and telecommunications infrastructure.

Hamza Gerçekcioğlu received the B.Sc. degree from Hacettepe University, Ankara, Türkiye, in 1996, and the M.Sc. and Ph.D. degrees from Gazi University, Ankara, in 2000 and 2008, respectively. His Ph.D. thesis is in the field of atmospheric turbulence and free space optics communication systems. Currently, he is with the Ministry of Transport and Infrastructure, Ankara. He was a Lecturer and a Researcher with the Department of Electronic Engineering, Kırıkkale University, in areas of communication systems, fiber optics, and telecommunication networks. He was a President with the Prime Ministry Undersecretaries for Maritime Affairs, Communications and Electronics Department; and managed Vessel Traffic Control and Infrastructure of Communications Systems of Turkish Territorial Waters. He was the Deputy Director General in the Ministry of Transport Maritime Affairs and Communications and the Directorate General of Aeronautics and Space Technologies. He has published several SCI journals and proceedings papers. With optical wave propagation in atmospheric and oceanic medium, his research interests include aerial vehicle and satellite laser and RF communications.

Yalçın Ata (Senior Member, IEEE) received the Ph.D. degree from Gazi University, Ankara, Türkiye, in 2010. From 2004 to 2020, he was a Senior Researcher, a Chief Researcher, and the Deputy Director of the TUBITAK Defense Industries Research and Development Institute and the TUBITAK Space Technologies Research Institute, Ankara, respectively. He is currently a Full Professor with the Electrical and Electronics Engineering Department, OSTIM Technical University, Ankara. His research interests include optical wireless communication, free-space optics, quantum communication, optical turbulence in atmosphere, underwater and biological tissue, and beam propagation in turbulent media.